Inorganic Chemistry

Article

pubs.acs.org/IC

# Syntheses, Characterization, and Optical Properties of Centrosymmetric $Ba_3(BS_3)_{1.5}(MS_3)_{0.5}$ and Noncentrosymmetric $Ba_3(BQ_3)(SbQ_3)$

Yan-Yan Li,[†,‡] Bing-Xuan Li,[†] Ge Zhang,[†] Liu-Jiang Zhou,[†] Hua Lin,[†] Jin-Ni Shen,[†,‡] Cheng-Yi Zhang,[†] Ling Chen,*[,†] and Li-Ming Wu*[,†]

[†]Key Laboratory of Optoelectronic Materials Chemistry and Physics, Fujian Institute of Research on the Structure of Matter, Chinese Academy of Sciences, Fuzhou, Fujian 350002, People's Republic of China

[‡]University of Chinese Academy of Sciences, Beijing 100039, People's Republic of China

Supporting Information

**ABSTRACT:** The most advanced UV−vis and IR NLO materials are usually borates and chalcogenides, respectively. But thioborates, especially thio-borometalates, are extremely rare. Here, four new such compounds are discovered by solid state reactions representing 0D structures constructed by isolated $BQ_3$ trigonal planes and discrete $MQ_3$ pyramids with $Ba^{2+}$ cations filling among them, centrosymmetric monoclinic $P2_1/c$ $Ba_3(BS_3)_{1.5}(MS_3)_{0.5}$ (M = Sb, Bi) **1**, **2** with $a$ = 12.9255(9), 12.946(2) Å; $b$ = 21.139(2), 21.170(2)Å; $c$ = 8.4194(6), 8.4207(8) Å; $\beta$ = 101.739(5), 101.688(7)°; $V$ = 2252.3(3), 2259.9(3) Å$^3$ and noncentrosymmetric hexagonal $P\bar{6}2m$ $Ba_3(BQ_3)(SbQ_3)$ (Q = S, Se) **3**, **4** with $a = b$ = 17.0560(9), 17.720(4) Å; $c$ = 10.9040(9), 11.251(3) Å; $V$ = 2747.1(3), 3060(2) Å$^3$. **3** exhibits the strongest SHG among thioborates that is about three times that of the benchmark $AgGaS_2$ at 2.05 $\mu$m. **1** and **3** also show an interesting structure relationship correlated to the size mismatching of the anionic building units that can be controlled by the experimental loading ratio of B:Sb. Syntheses, structure characterizations, and electronic structures based on the density functional theory calculations are reported.

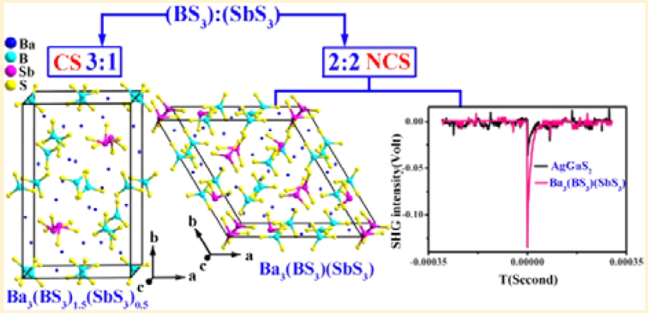


## INTRODUCTION

Nonlinear optical (NLO) materials have attracted great attention recently because of their potential applications in laser frequency conversion which can meet requirements in many fields.[1] According to their working spectral regions, borates are known as ultraviolet−visible NLO materials, such as the most advanced, commercially available benchmark $\beta$-$BaB_2O_4$ (BBO),[2] $LiB_3O_5$ (LBO);[3] and chalcogenides are classified as infrared (IR) NLO materials, such as the benchmark $AgGaS_2$,[4] $AgGaSe_2$.[5] Thioborates are thought to be an ideal system that can combine the favorable transparency and nonlinearity of sulfides with the high damage thresholds of borates.[6] To date, only a relatively small number of thioborates are structurally determined because of the high chemical reactivity of boron sulfide,[7] and most of them are centrosymmetric (CS). For example, seven ternary AE/B/S (AE = Ca, Sr, Ba) compounds are known as $CaB_2S_4$,[8] $SrB_2S_4$,[9] $Sr_3B_6S_{12}$,[10] $Sr_3B_2S_6$,[10] $Sr_{4.2}Ba_{2.8}B_4S_{13}$,[11] $BaB_2S_4$,[12] and $Ba_7B_4S_{13}$;[13] among them $BaB_2S_4$[12] is the only noncentrosymmetric (NCS) example. Similarly, very rare quaternary AE/B/M/S (M = transition or main group metals) compounds are known, and the only NCS compound $Zn_xBa_2B_2S_{5+x}$ ($x \approx 0.2$) exhibits a very weak second harmonic generation (SHG) efficiency (~50 times greater than that of $\alpha$-$SiO_2$ at 1.064 $\mu$m incident laser radiation).[6]

Among thioborates, the $[BS_3]^{3-}$ trigonal planar building unit is a common structural motif having strong polarization owning to the $\pi$-conjugated electrons delocalized on the plane that are very susceptible to the applied electric field. On the other hand, the $Sb^{3+}$ ion possessing stereochemically active lone pair electrons tends to form asymmetric building units, such as $SbS_3$ pyramid,[14] $SbS_4$ teeter-totter polyhedron,[15] $SbS_5$ square pyramid,[16] or $Sb_2S_5$ dimer.[17] We intend to combine these two units in a single crystal structure in order to construct a new NCS structure that may show desired NLO properties. Furthermore, the Ba/B/Sb/S system is less studied; a literature survey reveal one CS compound is known, namely $BaSb(BS_3)$.[18]

Herein, we discover four new compounds: centrosymmetric $Ba_3(BS_3)_{1.5}(SbS_3)_{0.5}$, **1**, $Ba_3(BS_3)_{1.5}(BiS_3)_{0.5}$, **2**, and noncentrosymmetric $Ba_3(BS_3)(SbS_3)$, **3**, $Ba_3(BSe_3)(SbSe_3)$, **4**. Remarkably, **3** exhibits the strongest SHG among thioborates that is about three times that of the benchmark $AgGaS_2$ at 2.05 $\mu$m.

**Received:** January 26, 2015
**Published:** April 30, 2015




DOI: 10.1021/acs.inorgchem.5b00189
*Inorg. Chem.* 2015, 54, 4761−4767

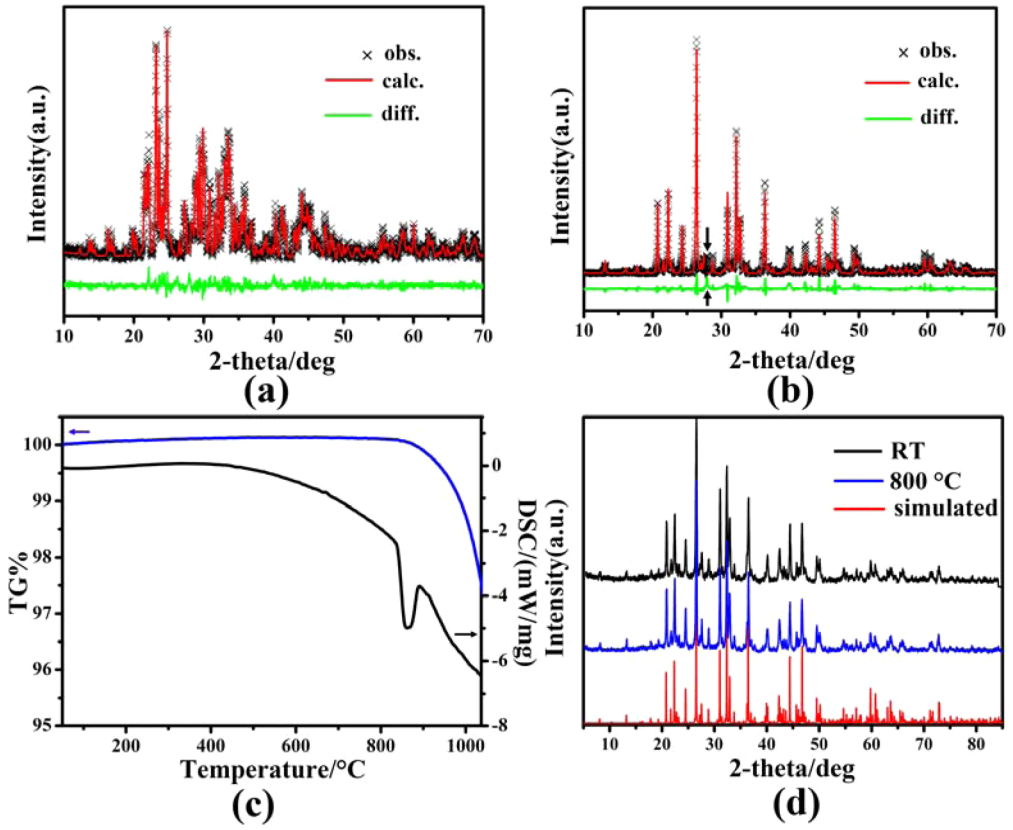


**Figure 1.** Experimental powder XRD (×), the calculated (solid line) and difference (bottom) results of the GSAS refinements for $Ba_3(BS_3)_{1.5}(SbS_3)_{0.5}$, **1** (a), and $Ba_3(BS_3)(SbS_3)$, **3** (b) (impurity of BaS in **3** is marked by the solid black arrow). (c) TG (blue) and DSC (black) diagrams of **3**. (d) X-ray powder diffraction patterns of manually picked crystals of **3** at room temperature (RT) or after being heated at 800 °C for 30 min under a constant flow of nitrogen gas.

Significantly, **1** and **3** illustrate a clearly centrosymmetric to noncentrosymmetric structure relationship correlated to the anion size mismatching. In addition, syntheses, structure characterizations, and electronic structures based on the density functional theory calculations are reported.

## EXPERIMENTAL SECTION

**Materials and Method.** All starting reactants were stored in an Ar-filled glovebox with controlled oxygen and moisture levels below 0.1 ppm, and all manipulations were carried out in the Ar-filled glovebox or under vacuum. The Ba (99.99%) purchased from Alfa Aesar China (Tianjin) Co., Ltd. was first brushed to remove the oxidized layer before being used in the synthesis. Sb block, Bi block, S powder, and Se powder (99.99% or higher) were purchased from Sinopharm Chemical Reagent Co., Ltd. Amorphous boron powder (95%−97%) was purchased from Dan Dong Chemical Industry. The mixture of pure elements in corresponding stoichiometric ratios was loaded into a graphite crucible, then sealed in an evacuated silica tube under vacuum $10^{-2}$ Pa, and heated in a tube furnace with controlled temperature.

**$Ba_3(BS_3)_{1.5}(MS_3)_{0.5}$ (M = Sb, Bi), 1, 2.** The light-yellow block-shaped crystal of **1** was first discovered by the reaction of Ba with B, Sb, and S in a 6:1:1:9 molar ratio with a total weight of about 300 mg. The reactants were heated to 920 °C in 30 h and held at this temperature for 100 h and then cooled to 300 °C at −5 °C/h before switching off the furnace. Carbon crucibles were used as containers to prevent boron sulfides reacting with silicon dioxide of the silica tube. Dark-yellow and block-shaped crystal of **2** is isostructural to **1** and was obtained similarly. Pure phases of **1** and **2** were synthesized by the stoichiometric mixtures of Ba, B, M (M = Sb, Bi), and S which were heated at 920 °C for 10 h (Figure 1a and Figure S1a in the Supporting Information). Crystal **1** is stable in the air for more than half a year, while crystal **2** gradually became black after several weeks.

**$Ba_3(BQ_3)(SbQ_3)$ (Q = S, Se), 3, 4.** The yellow block-shaped crystal **3** was obtained by heating a stoichiometric mixture of Ba, B, Sb, S (6:3:1:12) at 820 °C for 100 h which was subsequently cooled to 300 °C at −5 °C/h before switching off the furnace. Pure phase of compound **3** was explored by the stoichiometric mixtures of Ba, B, Sb, and S which were heated at 820 °C, and the 90% yield (based on Ba) of **3** with a small amount of BaS byproduct (about 10%) was obtained (Figure 1b). Besides, the crystal quality of **3** from the stoichiometric molar ratio was not as good as that from the original sample (elements ratio: Ba:B:Sb:S = 6:3:1:12; the highest reaction temperature: 820 °C) together with compounds **1** and BaS (see Supporting Information Figure S2). A mixture of compound **4** (about 85%) and byproduct BaSe (about 15%) was generated with stoichiometric mixtures of Ba, B, Sb, and Se under the following heating profile: heated to 840 °C in 30 h and held at this temperature for 16 h, then cooled to 700 °C at −7 °C/h and held at this temperature for 72 h, then cooled to 300 °C at −5.5 °C/h before switching off the furnace (see Supporting Information Figure S1b). This is the best result up to now, although only very tiny particles were obtained which limited the SHG measurement.

**Single Crystal X-ray Crystallography.** Single crystal X-ray diffraction data of these compounds were collected with the aid of a Mercury CCD automatic diffractometer equipped with a graphite-monochromated Mo K$\alpha$ radiation ($\lambda$ = 0.710 73 Å) at room temperature. The data were corrected for Lorentz and polarization factors. All of the four structures were solved by the direct methods and refined by the full-matrix least-squares fitting on $F^2$ by SHELX-97.[19]

Systematic absences, E-value statistics, and subsequent successful refinements of the collected data suggested that monoclinic $P2_1/c$ (no. 14, CS) was the only candidate space group for the two CS


DOI: 10.1021/acs.inorgchem.5b00189
Inorg. Chem. 2015, 54, 4761−4767

compounds **1** and **2**. All atoms of **1** and **2** were refined with anisotropic thermal parameters, and all positions were fully occupied. No missed symmetry elements were found after using the PLATON[20] program to check the final refined crystal structures of **1** and **2**.

Compound **3** was first refined without disorder with $R$ values of $R_1$ = 4.80% and $wR_2$ = 10.76% with one notable diffraction peak of 7.381 e/Å$^3$ and abnormal large atomic displacement parameter (ADP) of Sb1 (0.0596) that was about three times higher than those of other Sb sites (Sb2:0.0196, Sb3:0.0233). This might imply a possible partial occupancy. A free refinement gave an occupancy of 0.8803 on this Sb1 site with $R$ values of $R_1$ = 4.39% and $wR_2$ = 9.56% and a still high ADP for Sb1 (0.0493). Considering the similar coordination environment, the largest diffraction peak was thus assigned as Sb1′ atom, the site split partner of Sb1. The subsequent refinement gave normal ADP for Sb1 (0.0380) and better $R$ values of $R_1$ = 3.17% and $wR_2$ = 6.65% and occupancies of Sb1:0.8303 and Sb1′: 0.0849, respectively. The Flack parameter was 0.13(4), and a possible racemic twin was suggested. Then, a twin law −1 0 0, 0 −1 0, 0 0 −1 was used in the final refinement, which converged to $R_1$ = 3.17% and $wR_2$ = 6.62%, BASF of 0.1318, and a Flack parameter of 0.00(5). The subsequent PLATON[20] check suggested that the $P\bar{6}2m$ (no. 189, NCS) was a reliable space group. The experimental SHG of **3** confirmed the NCS symmetry of this compound. Compound **4** had been refined similarly with $R$ values of $R_1$ = 2.49% and $wR_2$ = 5.67%. Crystallographic data and structural refinement details are summarized in Table 1, and the positional coordinates together with isotropic equivalent thermal parameters of compounds **1**−**4** are given in Supporting Information Table S1. Some important bond distances and angles are respectively listed in Supporting Information Tables S2 and S3.

**Table 1. Crystal Data and Structure Refinements of $Ba_3(BS_3)_{1.5}(MS_3)_{0.5}$ (M = Sb, 1; Bi, 2) and $Ba_3(BQ_3)_3(SbQ_3)$ (Q = S, 3; Se, 4)**

| | formula | | | |
|---|---|---|---|---|
| | **1** | **2** | **3** | **4** |
| fw | 1362.94 | 1450.17 | 736.94 | 1018.34 |
| crystal system | monoclinic | monoclinic | hexagonal | hexagonal |
| crystal color | light-yellow | dark-yellow | yellow | red |
| space group | $P2_1/c$ (no.14) | $P2_1/c$ (no.14) | $P\bar{6}2m$ (no.189) | $P\bar{6}2m$ (no.189) |
| $a$ (Å) | 12.9255(9) | 12.946(2) | 17.0560(9) | 17.720(4) |
| $b$ (Å) | 21.139(2) | 21.170(2) | 17.0560(9) | 17.720(4) |
| $c$ (Å) | 8.4194(6) | 8.4207(8) | 10.9040(9) | 11.251(3) |
| $\alpha$ (deg) | 90 | 90 | 90 | 90 |
| $\beta$ (deg) | 101.739(5) | 101.688(7) | 90 | 90 |
| $\gamma$ (deg) | 90 | 90 | 120 | 120 |
| $V$ (Å$^3$) | 2252.3(3) | 2259.9(3) | 2747.1(3) | 3060(2) |
| $Z$ | 4 | 4 | 9 | 9 |
| $D_c$ (g.cm$^{-3}$) | 4.019 | 4.262 | 4.009 | 4.974 |
| $\mu$ (mm$^{-1}$) | 12.596 | 19.134 | 12.701 | 26.543 |
| GOOF on $F^2$ | 1.070 | 1.090 | 1.094 | 1.046 |
| $R_1$, $wR_2$ ($I > 2\sigma(I)$)[a] | 0.0249, 0.0448 | 0.0263, 0.0510 | 0.0317, 0.0656 | 0.0249, 0.0567 |
| $R_1$, $wR_2$ (all data) | 0.0297, 0.0469 | 0.0278, 0.0516 | 0.0328, 0.0686 | 0.0253, 0.0569 |
| largest diff. peak and hole (e/ Å$^3$) | 1.085, −0.954 | 1.992, −1.254 | 1.896, −1.919 | 1.770, −2.372 |
| Flack parameter | N/A | N/A | 0.00(5) | 0.00(2) |

[a] $R_1 = \Sigma||F_o| - |F_c||/\Sigma|F_o|$, $wR_2 = [\Sigma w(F_o^2 - F_c^2)^2/\Sigma w(F_o^2)^2]^{1/2}$.

**Powder X-ray Diffraction.** The powder X-ray diffraction data for finely ground samples were collected at 298 K on a Rigaku MiniFlex II diffractometer with Cu K$\alpha$ radiation in the 2$\theta$ range of 5−85° (Figure 1, Figure S1 and Figure S2 in the Supporting Information). Powder XRD data were analyzed using a profile fitting by a least-squares method employing the computer program GSAS implemented with EXPGUI.[21]

**Thermal Analysis.** Thermogravimetric analysis (TG) of the NLO active **3** was measured on a NETZSCH STA 449C simultaneous analyzer. Differential scanning calorimetry (DSC) of **3** was carried out on a NETZSCH DTA 404PC. Reference ($Al_2O_3$) and crystal samples (about 20 mg) were enclosed in $Al_2O_3$ crucibles and heated from room temperature to 1100 °C at a rate of 20 °C/min under a constant flow of nitrogen gas.

**Elemental Analysis.** The element ratio was measured by an energy dispersive X-ray spectroscope (EDX, Oxford INCA) on a field emission scanning electron microscope (FESEM, JSM6700F) for polycrystalline **1**−**4** (Supporting Information Figure S3; Table S4). The Ba/Sb/S molar ratio was measured to be approximately 2.77:0.5:5.63 (**1**); Ba/Bi/S = 2.86:0.5:6.34 (**2**); Ba/Sb/S = 2.70:1:5.90 (**3**); and Ba/Sb/Se = 2.86:1:5.67 (**4**). The quantitative inductively coupled plasma (ICP) emission spectra examined with the aid of an Ultima-2 inductively coupled plasma emission spectrometer (ICP-OES) gave mass percentages of 59.33% Ba, 2.66% B, and 9.41% Sb for **1**, 53.64% Ba, 2.06% B, and 16.17% Bi for **2**, 53.72% Ba, 1.21% B, and 17.63% Sb for **3**, and 38.65% Ba, 0.96% B, 12.05% Sb, and 42.82% Se for **4**, respectively (Supporting Information Table S4). The results of EDX and ICP were in good agreement with those established by single crystal diffraction data (Table 1, and Table S1 in the Supporting Information).

**IR and Raman Spectroscopy.** The IR spectra were measured by a Nicolet Magana 750 FT-IR spectrophotometer in the range of 400−1200 cm$^{-1}$ for **1**, **2** and 2.5−25 $\mu$m for **3**. Polycrystalline samples were ground with KBr and pressed into the form of transparent pellets for spectrum measurement.

The Raman spectra of **1** and **2** were recorded with a confocal Raman microspectrometer (invia-Reflex, Renishaw, Great Britain) in the range of 200−1200 cm$^{-1}$ by a 532 nm diode laser excitation at 298 K.

**UV−Vis−NIR Diffuse Reflectance Spectra.** The optical diffuse reflectance spectra of powder samples in the range of 0.19−2.5 $\mu$m were recorded at room temperature using a PerkinElmer Lambda 900 UV−vis spectrophotometer equipped with an integrating sphere attachment. $BaSO_4$ plate was used as a reference, on which the finely ground powders of the samples were coated. The absorption spectrum was calculated from the diffuse reflection spectrum via the Kubelka−Munk function: $\alpha/S = (1 - R)^2/2R$, in which $\alpha$, $S$, $R$ are the absorption coefficient, the scattering coefficient, and the reflectance, respectively.[22]

**Powder Second Harmonic Generation (SHG) Measurements.** The SHG of **3** were measured on a modified Kurtz-NLO system using a 2.05 $\mu$m laser radiation with a photomultiplier as the detector of the output signal.[23] Manually picked crystals of **3** were ground and sieved in the range of 30−46 $\mu$m and were pressed into a disk with diameter of 8 mm, which was put between glass microscope slides and secured with tape in a 1 mm thick aluminum holder. Larger $AgGaS_2$ crystals were crushed, ground, and sieved into the same size range and were used as the reference.

**Computational Section.** The band structures were calculated by the Vienna ab initio simulation package (VASP).[24] The generalized gradient approximation (GGA)[25] was chosen as the exchange-correlation functional, and a plane-wave basis with the projector augmented wave (PAW)[26] potentials was used. The plane-wave cutoff energy of 400 eV and the threshold of $10^{-5}$eV were set for the self-consistent-field convergence of the total electronic energy, and the Fermi level ($E_f$ = 0 eV) was selected as the reference of the energy. The electronic configurations for B, S, Se, Sb, Bi, and Ba were $2s^22p^1$, $3s^23p^4$, $4s^24p^4$, $5s^25p^3$, $5d^{10}6s^26p^3$, and $5s^25p^66s^2$, respectively. For compounds **3** and **4**, the calculation model was built in $P1$ symmetry. The $k$ integrations over the Brillouin were performed by using 5 × 3 × 7 and 3 × 3 × 5 Monkhorst−Pack $k$-points for compounds **1**, **2** and **3**, **4**, respectively. In the geometrical optimizations, the quasi-newton minimization method was employed to make sure that the Hellmann−Feynman force on each atom was less than 0.02 eV/Å.



DOI: 10.1021/acs.inorgchem.5b00189
Inorg. Chem. 2015, 54, 4761−4767

More than 200 empty bands were used in the optical property calculations, and scissors operators of 0.67 eV were applied for compound **3**. The dielectric function $\varepsilon(\omega) = \varepsilon_1(\omega) + i\varepsilon_2(\omega)$ was first calculated, of which the imaginary part $\varepsilon_2(\omega)$ could be obtained from the Kubo–Greenwood formula,[27] and the real part $\varepsilon_1(\omega)$ was deduced from the Kramer–Kronig relationship.[28,29] All the other linear optical constants could be also derived from $\varepsilon_2(\omega)$ from Kramer–Kronig transform. The static and dynamic second-order nonlinear susceptibilities $\chi^{abc}$ $(-2\omega, \omega, \omega)$ were calculated based on the so-called length-gauge formalism by Aversa and Sipe.[30,31]

## RESULTS AND DISCUSSION

**1. Centrosymmetric $Ba_3(BS_3)_{1.5}(MS_3)_{0.5}$ (M = Sb, Bi) 1, 2.** Compounds **1** and **2** crystallize in the monoclinic CS space group $P2_1/c$ (no. 14) with a Pearson's symbol of $mP88$.

Crystal **1** represents a 0D structure constructed by isolated $[BS_3]^{3-}$ trigonal planes and discrete $[SbS_3]^{3-}$ pyramids with $Ba^{2+}$ cations filling among them (Figure 2a), Each boron atom has a trigonal plane coordination with three sulfide atoms, and B–S bond lengths range from 1.781(6) to 1.829(6) Å, which are typical and in accordance with those in $BaB_2S_4$[12] and $Sr_{4.2}Ba_{2.8}B_4S_{13}$.[11] The distortions of the $[BS_3]^{3-}$ trigonal planes are evidenced by deviations of both B–S bonds (1.781(6)–1.829(6) Å) and S–B–S angles (116.9(3)–123.4(3)°). Characteristically, these polarized $[BS_3]^{3-}$ trigonal planes exhibit delocalized $\pi$-bonding formed by the nonbonding $p_z$-orbitals of every S atom that are perpendicular to the trigonal plane. Nevertheless, the overall polarities of $[BS_3]^{3-}$ units are canceled by the inversion center symmetry operation.

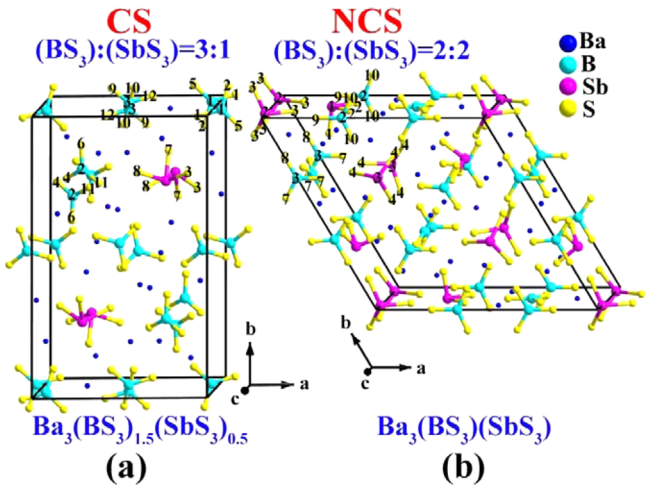


**Figure 2.** Structures with unit cell marked of (a) $Ba_3(BS_3)_{1.5}(SbS_3)_{0.5}$, **1**; (b) $Ba_3(BS_3)(SbS_3)$, **3**. Blue, Ba; purple, Sb; bright cyan, B; yellow, S.

The discrete $[SbS_3]^{3-}$ pyramid is also distorted owing to the stereochemically active lone pair electrons on $Sb^{3+}$, which is evidenced by deviations of both Sb–S bonds (2.447(2)–2.484(2) Å) and S–Sb–S angles (92.08(5)–100.22(5)°). Along the $a$ axis, $[SbS_3]^{3-}$ trigonal pyramids are aligned linearly, as those in $Tl_3SbS_3$[32] (Supporting Information Figure S4). Because of the centrosymmetry, the individual polarities of such pyramids are canceled by the same kind of neighboring species. The mean Sb–S bond length (2.4597 Å) of $[SbS_3]^{3-}$ agrees well with that in $PbAgSbS_3$ (2.4547 Å).[33] The S–Sb–S angle deviation in **1** is comparable with those in $Ba_8Sb_6S_{17}$ (92.813–101.210°),[34] but smaller than that in $BaBSbS_4$ (76.50–97.73°).[18]

The Ba1, Ba2, Ba4, Ba6 ions are eightfold coordinated to S atoms, and Ba3, Ba5 are ninefold coordinated to S atoms, respectively. The Ba–S distances varying from 3.097(2) to 3.512(2) Å are consistent with those in $Ba_3Sb_{4.667}S_{10}$[35] (Supporting Information Figure S5).

**2. Noncentrosymmetric $Ba_3(BQ_3)(SbQ_3)$ (M = S, Se) 3, 4.** Compounds **3** and **4** crystallize in the hexagonal NCS $P\bar{6}2m$ (no. 189). The same as **1**, compound **3** is also a 0D structure constructed by isolated $[BS_3]^{3-}$ trigonal planes and discrete $[SbS_3]^{3-}$ pyramids (Figure 2b), Every two isolated $[Sb2S_3]^{3-}$ or $[Sb3S_3]^{3-}$ pyramids along the $c$ axis are antialigned. The Sb–S bond lengths of such pyramids are 2.448(3) and 2.446(2) Å, which are typical and are in accordance with those in $Ag_3SbS_3$ (Sb–S: 2.444 Å).[36] The B1 located at 3$g$ site and B2, B3 located at 3$f$ site with $m2m$ site symmetry are in typical trigonal plane coordination with 3 S atoms and bond lengths ranging from 1.772(8) to 1.96(2) Å, in accordance with those in **1**.

The Sb1 (occu.: 0.830(2), Wyckoff site 3$g$) atom has a pyramidal geometry which is coordinated to 2 S2 (Sb1–S2:2.427(4)) and 1 S1 atom which is equally split into two positions (Supporting Information Figure S6). A similar situation is seen in $Pb_{28}As_5Sb_7S_{46}$.[37]

The Ba cations exhibit typical eight- or ninefold coordination with Ba–S bond length ranging from 3.105(2) to 3.488(2) Å (Supporting Information Figure S7).

**3. Structure Comparison among $Ba_3(BS_3)_{1.5}(SbS_3)_{0.5}$, 1, $Ba_3(BS_3)(SbS_3)$, 3, and $BaSb(BS_3)S$,[18] 5.** These three compounds are formed by the same components, yet their structures are totally different: **5** is a CS 1D chain structure[18] (Supporting Information Figure S8a), **1** is a CS 0D, and **3** is a NCS 0D structure. It is generally accepted that as the Ba content increases from 33.3% (**5**) to 60% (**1**, **3**), the dimensionality decreases from 1D (**5**) to 0D (**1**, **3**). Also, involving more ionic $Ba^{2+}$ cations in the latter separates the building units further apart, which is reflected by the distance between the nearest neighboring building units. As such, the two most adjacent $SbS_3$ and $BS_3$ units in **5** are joined by S1 atom and are 3.202 Å apart roughly judging by the Sb–S3 distance (Supporting Information Figure S8a). However, in **1**, these units are further apart, e.g., the $SbS_3$ unit is 4.2 Å away from the B1$S_3$ unit (indicated by Sb–S2 = 4.162 Å) and 4.1 Å away from the B3$S_3$ unit (indicated by Sb–S9 = 4.136 Å) and about 3.6 Å apart from the neighboring $SbS_3$ unit (the intraunit Sb–S distances are 3.621 and 3.586 Å) (Supporting Information Figure S8b). Different from this, the structure change between **1** and **3** is of interest. From their formula, **1** and **3** have the same number of Ba cations and S anions, only differing in the ratio of $BS_3/SbS_3$, i.e., B:Sb = 3:1 and 2:2, respectively. Such a ratio influences the formation of the NCS structure. We believe the reason is that B (a period 2 element) is significantly smaller in size than Sb (a period 5 element) and having the same amount of $BS_3$ and $SbS_3$ in **3** strengthens the size mismatch between the two building units, which evidently make the formation of a NCS structure possible.

**Thermal Stabilities.** The TG and DSC measurement results indicate that **3** is thermally stable up to at least 800 °C under a $N_2$ atmosphere (Figure 1c). Right after the DSC measurement under 800 °C for half an hour, the same sample was checked by X-ray powder diffraction. The data indicate it as a pure phase identical to that before the measurement (Figure 1d).

**Infrared and Raman Scattering Spectra.** Infrared and Raman spectra were collected for **1** and **2** to probe the presence


DOI: 10.1021/acs.inorgchem.5b00189
Inorg. Chem. 2015, 54, 4761–4767

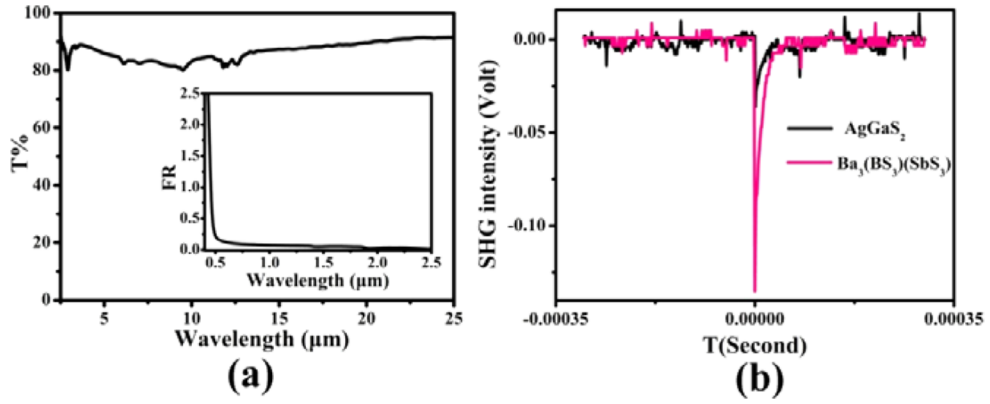


**Figure 3.** (a) Reflection spectra and FT-IR spectra of $Ba_3(BS_3)(SbS_3)$, **3**. (b) Oscilloscope traces of SHG signals of $Ba_3(BS_3)(SbS_3)$, **3**, and $AgGaS_2$ (reference) in the particle size of 30−46 $\mu$m.

of lighter element boron via the characteristic vibrational information on $[BS_3]^{3-}$ groups. As shown in Supporting Information Figures S9, S10, the relatively strong absorption bands in the Infrared spectra and the weak absorption bands in the Raman spectra from 800 to 900 $cm^{-1}$ are assigned to the E asymmetrical stretching modes of $[BS_3]^{3-}$.[6] The weak absorption bands in the infrared spectra and the relatively strong absorption bands in the Raman spectra from 415 to 445 $cm^{-1}$ are assigned to the A1 symmetrical stretching modes of the $[BS_3]^{3-}$ units.[38] Similar absorption bands are observed in $Na_3BS_3$[39] and $Ba_7B_4S_{13}$.[13] It should be mentioned that the presence of splitting vibration modes around 850 $cm^{-1}$ is caused by the deviations of both B−S distance (1.78−1.83 Å) and S−B−S angle (116−124°) in the $[BS_3]^{3-}$ unit which reduces the symmetry from $D_{3h}$ to $C_{2v}$.[18] Additionally, the strong absorption bands in the Raman spectra from 220 to 339 $cm^{-1}$ are assigned to the internal vibrations (the stretching and bending modes) of the $[SbS_3]^{3-}$ pyramids in **1**. In **2**, the internal vibrations of $[BiS_3]^{3-}$ pyramids occur at ∼150−280 $cm^{-1}$. Similar absorption bands are reported previously.[40]

Compound **3** is almost transparent in the range of 2.5−11 and 13−25 $\mu$m (Figure 3a). The absorptions from 11.76 to 12.50 $\mu$m (about 800−850 $cm^{-1}$) belong to the E asymmetrical stretching modes of $[BS_3]^{3-}$ unit. Those peaks at ∼2.90, 6.12, and 9.53 $\mu$m (i.e., 1049, 1633, 3448 $cm^{-1}$) are the remains which are not fully subtracted from the background similar to those in $Ba_2BiInS_5$.[41]

**UV/Vis/NIR Absorption.** In agreement with their light-yellow, dark-yellow, yellow, and red colors, respectively, the optical band gaps of compounds **1**−**4** are measured to be approximately 3.01, 2.43, 2.62, and 1.89 eV (Supporting Information Figure S11a), whereas the calculated band gaps are 2.60, 2.57, 1.95, and 1.44 eV (Figure 4 and Supporting Information Figure S12).

**Second Harmonic Generation (SHG) Property.** The SHG of polycrystalline $Ba_3(BS_3)(SbS_3)$, **3** is roughly three times that of $AgGaS_2$ at the particle size of 30−46 $\mu$m, the strongest response among thioborates to date (Figure 3b). Some relevant examples only show weak SHG intensity, such as $Zn_xBa_2B_2S_{5+x}$ ($x \approx 0.2$),[6] 50 × $\alpha$-$SiO_2$; (KBr) $[SmB_{12}(GaS_4)_3]$,[42] 0.3 × KDP ($KH_2PO_4$).

The band gap of **3** (2.62 eV) is slightly larger than that of the commercial $AgGaS_2$ (2.56 eV, Supporting Information Figure S11b), which indicates that **3** may have similar laser-induced damage threshold. Generally compounds having wider band gaps tend to show higher laser-induced damage threshold.

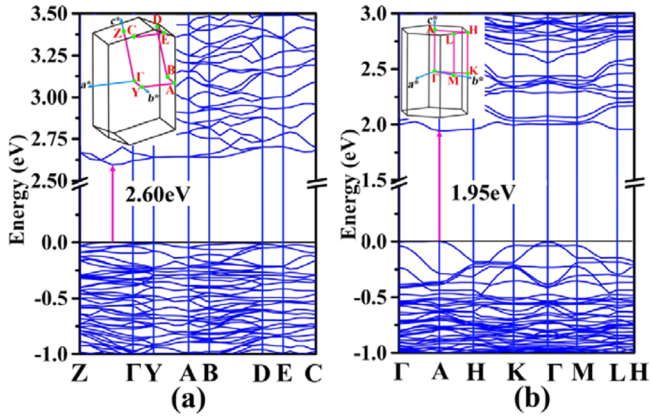


**Figure 4.** Calculated band structures of (a) $Ba_3(BS_3)_{1.5}(SbS_3)_{0.5}$, **1**, and (b) $Ba_3(BS_3)(SbS_3)$, **3**. The inset figures are the first Brillouin zones (BZ) with the high-symmetry points (bright green point) and lines (red line).

Thus, involving B in sulfidoantimonates may improve the laser-induced damage threshold for band gaps of $Ba_3(BS_3)_{1.5}(SbS_3)_{0.5}$ (**1**, 3.01 eV), $Ba_3(BS_3)(SbS_3)$ (**3**, 2.62 eV), and $BaSb(BS_3)S$ (2.70 eV)[18] are larger than that of $Ba_3Sb_{4.667}S_{10}$ (2.14 eV).[35] Meanwhile, compound **3** shows a transparent range of about 0.5−25 $\mu$m except for several absorption bands at 11.76−12.50 $\mu$m that are caused by the $[BS_3]^{3-}$ unit (Figure 3a). This is broadened compared to that of commercial $AgGaS_2$ (∼0.7−23 $\mu$m) at both the visible and infrared regions (Supporting Information Figure S11b).

**Electronic Structure and Linear and Nonlinear Optical Property Studies.** The band structures of **1** and **3** are shown in Figure 4, which reveals direct band gaps of 2.60 and 1.95 eV, respectively. (The electronic structures of **2**, **4** are shown in Supporting Information Figures S12 and S13.) The DOS shown in Figure 5 shows that the top of the valence band (VB) of **1**, **3** contains mainly S-3p and Ba-5d states with some contributions of Ba-5p and B-2p. The S-3p strongly hybridizes with Sb-5p and B-2p from −4.0 to −2.0 eV. Above the Fermi level, conduction bands are dominated by B-2p, Sb-5p, and Ba-5d states. Thus, the electronic transitions are mainly from S-3p states to B-2p, Sb-5p, and Ba-5d states.

The linear and nonlinear optical properties of **3** are also calculated. The frequency-dependent dielectric functions including calculated imaginary $\varepsilon_2(\omega)$ and real $\varepsilon_1(\omega)$ are shown in Supporting Information Figure S14. The average


DOI: 10.1021/acs.inorgchem.5b00189
Inorg. Chem. 2015, 54, 4761−4767

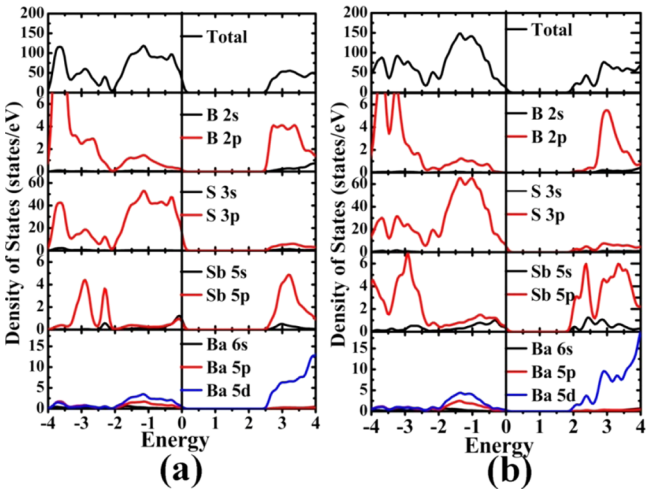


**Figure 5.** Total and partial density of states: (a) $Ba_3(BS_3)_{1.5}(SbS_3)_{0.5}$, **1**; (b) $Ba_3(BS_3)(SbS_3)$, **3**.

value of the polarized zero-frequency dielectric constants $\varepsilon_1^{ave}(0)$ is 4.62. The main peaks of imaginary part $\varepsilon_2(\omega)$ are located around 6.5 eV, which can be mainly regarded as electronic interband transitions from the S-3p to B-2p and Sb-5p states. The birefringence ($\Delta n$) was also calculated and shown in Supporting Information Figure S15. The static birefringence is 0.05, which is close to $AgGaS_2$ (0.039),[43] indicating **3** may achieve a phase-matchable condition.

The space group of **3** is $P\bar{6}2m$ of the class 3 and has one independent nonvanishing second-order susceptibility tensor ($d_{21}$) ($d_{21} = -d_{22}$). Because of the disorder of Sb and S atoms in **3**, a model with *P*1 symmetry was built, which had 10 independent second-order tensors under the restriction of Kleinman symmetry ($d_{11}$, $d_{12}$, $d_{13}$, $d_{14}$, $d_{15}$, $d_{16}$, $d_{22}$, $d_{23}$, $d_{24}$, and $d_{33}$). Among them, $d_{21}$ was studied. As shown in Supporting Information Figure S16a, the calculated $d_{21}$ ($-d_{22}$) coefficient for **3** is 2.73 pm/V at the wavelength of 2.05 $\mu$m (0.61 eV).

The cutoff-energy-dependent second-order coefficient $d_{21}$ ($-d_{22}$) has been presented to understand the origin of the SHG components of **3**, as plotted in Supporting Information Figure S16b. Regions 1−3 mainly contribute to the SHG. The region-1 is dominated by S-3p states hybridized with a small amount of B-2p and Sb-5p. Region-2 has main contributions from B-2p and Sb-5p states with small amounts of S-3p, while region-3 mainly consists of Sb-5p states with small amounts of Ba-5d. Thus, the SHG should be ascribed to the transition process from S-3p to B-2p, Sb-5p and Ba-5d states.

## CONCLUSIONS

In summary, four new zero-dimensional (0D) compounds, centrosymmetric $Ba_3(BS_3)_{1.5}(MS_3)_{0.5}$ (M = Sb, Bi) **1**, **2**, and noncentrosymmetric $Ba_3(BQ_3)(SbQ_3)$ (M = S, Se) **3**, **4** are discovered by solid state reactions. Polycrystalline **3** exhibits the strongest SHG among thioborates, about three times as large as that of the benchmark $AgGaS_2$ in the same particle size. **1** and **3** also show an interesting centrosymmetric-to-noncentrosymmetric structure relationship correlated to the size mismatching of the anionic building units that can be controlled by the experimental loading ratio of B:Sb. Such an insight may shed useful light on the future studies on the design synthesis of the desired noncenstrosymmetric compounds in this and related systems. Further studies are worthwhile.

## ASSOCIATED CONTENT

### Supporting Information

The cif files, additional tables, and figures. The Supporting Information is available free of charge on the ACS Publications website at DOI: 10.1021/acs.inorgchem.5b00189.

## AUTHOR INFORMATION

### Corresponding Authors

*E-mail: chenl@fjirsm.ac.cn.

*E-mail: liming_wu@fjirsm.ac.cn. Tel.: (011)86-591-63173211.

### Notes

The authors declare no competing financial interest.

## ACKNOWLEDGMENTS

This work was supported by the National Natural Science Foundation of China under Projects 21233009, 21225104, 91422303, 21301175 and 21171168.

## REFERENCES

(1) (a) Wu, X. T.; Chen, L., Vol. Eds. *Structure−Property Relationships in Non-Linear Optical Crystals. I. The UV-Vis Region*. In *Struct. Bonding (Berlin)*; Mingos, D. M. P., Series Ed.; Springer: New York, 2012; Vol. *144*. (b) Wu, X. T.; Chen, L., Vol. Eds. *Structure−Property Relationships in Nonlinear Optical Crystals. II. The IR Region*. In *Struct. Bonding (Berlin)*; Mingos, D. M. P., Series Ed.; Springer: New York, 2012; Vol. *145*.

(2) Chen, C. T.; Wu, B. C.; Jiang, A. D.; You, G. M. *Sci. Sin., Ser. B* **1985**, *28*, 235−240.

(3) Chen, C. T.; Wu, Y. C.; Jiang, A. D.; Wu, B. C.; You, G. M.; Li, R. K.; Lin, S. J. *J. Opt. Soc. Am. B* **1989**, *6*, 616−621.

(4) (a) Jayaraman, A.; Narayanamurti, V.; Kasper, H. M.; Chin, M. A.; Maines, R. G. *Phys. Rev. B* **1976**, *14*, 3516−3519. (b) Harasaki, A.; Kato, K. *Jpn. J. Appl. Phys.* **1997**, *36*, 700−703.

(5) Catella, G. C.; Shiozawa, L. R.; Hietanen, J. R.; Eckardt, R. C.; Route, R. K.; Feigelson, R. S.; Cooper, D. G.; Marquardt, C. L. *Appl. Opt.* **1993**, *32*, 3948−3951.

(6) Kim, Y.; Martin, S. W.; Ok, K. M.; Halasyamani, P. S. *Chem. Mater.* **2005**, *17*, 2046−2051.

(7) Krebs, B. *Phosphorus, Sulfur Silicon Relat. Elem.* **2001**, *168*, 11−22.

(8) Sasaki, T.; Takizawa, H.; Takeda, T.; Endo, T. *Mater. Res. Bull.* **2003**, *38*, 33−39.

(9) Püttmann, C.; Hamann, W.; Krebs, B. *Eur. J. Solid State Inorg. Chem.* **1992**, *29*, 857−872.

(10) Hammerschmidt, A.; Döch, M.; Püttmann, C.; Krebs, B. *Z. Anorg. Allg. Chem.* **2003**, *629*, 551−555.

(11) Hammerschmidt, A.; Köster, C.; Küper, J.; Lindemann, A.; Krebs, B. *Z. Anorg. Allg. Chem.* **2001**, *627*, 1253−1258.

(12) Hammerschmidt, A.; Döch, M.; Wulff, M.; Krebs, B. *Z. Anorg. Allg. Chem.* **2002**, *628*, 2637−2640.

(13) Kim, Y.; Martin, S. W. *Inorg. Chem.* **2004**, *43*, 2773−2775.

(14) Chen, M. C.; Wu, L. M.; Lin, H.; Zhou, L. J.; Chen, L. *J. Am. Chem. Soc.* **2012**, *134*, 6058−6060.

(15) Zhao, H. J.; Li, L. H.; Wu, L. M.; Chen, L. *Inorg. Chem.* **2009**, *48*, 11518−11524.

(16) Zhao, H. J.; Li, L. H.; Wu, L. M.; Chen, L. *Inorg. Chem.* **2010**, *49*, 5811−5817.

(17) Chen, M. C.; Li, L. H.; Chen, Y. B.; Chen, L. *J. Am. Chem. Soc.* **2011**, *133*, 4617−4624.

(18) Geng, L.; Cheng, W. D.; Zhang, W. L.; Lin, C. S.; Zhang, H.; Li, Y. Y.; He, Z. Z. *Inorg. Chem.* **2010**, *49*, 6609−6615.

(19) Sheldrick, G. M. *SHELXTL*, version 5.1; Bruker-AXS: Madison, WI, 1998.

(20) Spek, A. L. *J. Appl. Crystallogr.* **2003**, *36*, 7−13.

(21) Toby, B. H. *J. Appl. Crystallogr.* **2001**, *34*, 210−213.

(22) Kortüm, G. *Reflectance Spectroscopy*; Springer-Verlag: New York, 1969.



DOI: 10.1021/acs.inorgchem.5b00189
*Inorg. Chem.* 2015, 54, 4761−4767

(23) (a) Kurtz, S. K.; Perry, T. T. *J. Appl. Phys.* **1968**, *39*, 3798−3813. (b) Lin, X. S.; Zhang, G.; Ye, N. *Cryst. Growth Des.* **2009**, *9*, 1186−1189. (c) Huang, Y. Z.; Wu, L. M.; Wu, X. T.; Li, L. H.; Chen, L.; Zhang, Y. F. *J. Am. Chem. Soc.* **2010**, *132*, 12788−12789.
(24) Kresse, G.; Furthmüller, J. *Phys. Rev. B* **1996**, *54*, 11169−11186.
(25) Perdew, J. P.; Wang, Y. *Phys. Rev. B* **1992**, *45*, 13244−13249.
(26) (a) Kresse, G.; Joubert, D. *Phys. Rev. B* **1999**, *59*, 1758−1775. (b) Blöchl, P. E. *Phys. Rev. B* **1994**, *50*, 17953−17979.
(27) Ching, W. Y. *J. Am. Ceram. Soc.* **1990**, *73*, 3135−3160.
(28) Laksari, S.; Chahed, A.; Abbouni, N.; Benhelal, O.; Abbar, B. *Comput. Mater. Sci.* **2006**, *38*, 223−230.
(29) Mo, S. D.; Ching, W. Y. *Phys. Rev. B* **1995**, *51*, 13023−13032.
(30) Aversa, C.; Sipe, J. E. *Phys. Rev. B* **1995**, *52*, 14636−14645.
(31) Rashkeev, S. N.; Lambrecht, W. R. L.; Segall, B. *Phys. Rev. B* **1998**, *57*, 3905−3919.
(32) Kharbish, S. *Am. Mineral.* **2011**, *96*, 609−616.
(33) Ito, T.; Nowacki, W. *Z. Kristallogr.* **1974**, *139*, 85−102.
(34) Dörrscheidt, W.; Schäfer, H. *Z. Naturforsch., B* **1981**, *36*, 410−414.
(35) Choi, K. S.; Kanatzidis, M. G. *Inorg. Chem.* **2000**, *39*, 5655−5662.
(36) Laufek, F.; Sejkora, J.; Dušek, M. *J. Geosci.* **2010**, *55*, 161−167.
(37) Birnie, R. W.; Burnham, C. W. *Am. Mineral.* **1976**, *61*, 963−970.
(38) (a) Royle, M.; Cho, J.; Martin, S. W. *J. Non-Cryst. Solids.* **2001**, *279*, 97−109. (b) Cho, J.; Martin, S. W. *J. Non-Cryst. Solids.* **2002**, *298*, 176−192.
(39) Kuchinke, J.; Jansen, C.; Lindemann, A.; Krebs, B. *Z. Anorg. Allg. Chem.* **2001**, *627*, 896−902.
(40) Kharbish, S.; Libowitzky, E.; Beran, A. *Eur. J. Mineral.* **2009**, *21*, 325−333.
(41) Geng, L.; Cheng, W. D.; Lin, C. S.; Zhang, W. L.; He, Z. Z. *Inorg. Chem.* **2011**, *50*, 5679−5686.
(42) Guo, S. P.; Guo, G. C.; Wang, M. S.; Zou, J. P.; Zeng, H. Y.; Cai, L. Z.; Huang, J. S. *Chem. Commun.* **2009**, 4366−4368.
(43) Lin, H.; Zhou, L. J.; Chen, L. *Chem. Mater.* **2012**, *24*, 3406−3414.



DOI: 10.1021/acs.inorgchem.5b00189
*Inorg. Chem.* 2015, 54, 4761−4767